forests

MDPI

Article

Preliminary Metrological Characterization of Low-Cost MEMS Inclinometer for Tree Stability Assessment: From Laboratory to Field

Ilaria Incollu [1,*], Francesca Giannetti [2,3,4], Yamuna Giambastiani [2,4], Andrea Giachetti [5], Hervè Atsè Corti [2], Tommaso Tognetti [2], Gianni Bartoli [5] and Filippo Giadrossich [1]

[1] Department of Agricultural Sciences, University of Sassari, 07100 Sassari, Italy
[2] Bluebiloba Startup Innovativa SRL, 50126 Florence, Italy
[3] Geolab Laboratory of Forest Geomatics, Department of Agriculture, Food, Environment and Forestry, University of Florence, 50145 Florence, Italy
[4] ForTech Laboratorio Congiunto, University of Florence, 50145 Florence, Italy
[5] Department of Civil and Environmental Engineering, University of Florence, 50126 Florence, Italy
* Correspondence: i.incollu@phd.uniss.it

Abstract

Urban trees provide important benefits but can also pose safety risks when stability is reduced. Visual Tree Assessment (VTA) is typically the first step in risk analysis and is sometimes complemented by instrumental methods such as dynamic and static tests. Static pulling tests provide quantitative information on anchorage, but their cost and logistics limit use to site-specific applications. This study evaluates a low-cost Micro-Electro-Mechanical Systems (MEMS) inclinometer for quasi-static inclination measurements during a static pulling test, combining a laboratory calibration against a geometric reference with field comparisons against a professional high-precision inclinometer commonly used in static pulling tests. In the laboratory, using a calibrated tilting beam and a 120 s averaging window, the MEMS sensor yielded absolute errors on the order of a few hundredths of a degree (up to ≈0.015°) compared to the geometric expectation. In the field, comparisons were performed in the relative domain (baseline on the first stable plateau) along the longitudinal component, showing high concordance with the reference high-precision inclinometer commonly used in arboricultural pulling tests (e.g., $r \geq 0.99$, RMSE ≈ 0.04–0.07°, Deming slope ≈ 1.02–1.05). These results support the feasibility of low-cost MEMS for static tilt assessment. Given battery-powered wireless operation and simple processing, they indicate a potential for wider deployments in repeated or scheduled quasi-static assessments (e.g., during controlled pulling tests), complementing professional instrumentation.

Keywords: MEMS inclinometer; tree stability; static pulling test; low-cost sensors; urban forestry

Check for updates

Academic Editors: Jianping Wu, Zhongbing Chang, Xin Xiong and Jianling Li

Received: 13 January 2026
Revised: 6 February 2026
Accepted: 11 February 2026
Published: 13 February 2026

Copyright: © 2026 by the authors. Licensee MDPI, Basel, Switzerland. This article is an open access article distributed under the terms and conditions of the Creative Commons Attribution (CC BY) license.

1. Introduction

Urban trees are widely recognized for the multiple ecosystem services they provide, such as improving air quality and sequestering carbon [1–4]. They also regulate local microclimates through shading, evapotranspiration, and altered airflow patterns [5–9]; however, their presence could also be associated with potential disservices [10,11]. Among these, structural instability-related safety hazards pose a significant concern, with direct implications for both people and infrastructure [12–15]. A recent study from the Netherlands

highlighted the magnitude of the problem, reporting an average of 1.5–2 fatalities per year associated with tree failures in the Netherlands, corresponding to an individual annual risk of roughly 1 in 1,000,000 [13]. In Italy, a recent study by Buson et al. [12] indicated a growing number of emergency interventions for hazardous fallen trees, increasing from approximately 3500 in 2014 to almost 68,000 in 2023; in 2021 alone, more than 28,000 trees were removed in provincial capitals, with 77% classified as dangerous [12,16,17]. For these reasons, municipalities are faced with the complex task of preserving the benefits of trees while simultaneously adopting proactive strategies to minimize the risk of failure in densely populated contexts [18].

To address these challenges, municipalities and urban forest managers adopt risk assessment procedures to ensure the safety and health of urban trees [18,19]. These procedures commonly rely on the Visual Tree Assessment (VTA) method [20], often complemented by instrumental techniques, such as sonic tomography, wood resistance measurements to assess wood density, and pulling tests to evaluate tree stability [19,21]. Among the available methods for assessing tree stability, instrumental approaches, including dynamic sway assessment and pulling tests [15,22–24], provide valuable insights. In particular, static pulling tests have emerged as a widely adopted non-destructive technique for estimating root anchorage strength, based on the measurement of basal inclination under controlled loads [23,25–27], and further refined through coupling with mechanical modelling to quantify the root–soil anchorage behaviour under sustained loading [28]. Several studies have confirmed the effectiveness of pulling tests for providing reliable stability diagnostic data [29–31]. However, the high costs of professional instrumentation and the logistical effort required for each test make it challenging to apply this methodology on a large scale for frequent, repeated assessments across extensive urban tree populations [21].

Tree stability can be investigated through two complementary tree assessment approaches: pulling tests, directly related to the integrity of the root-soil anchorage [23,32], and dynamic analysis, which provides information on oscillation properties such as natural frequency and damping ratio [24]. Continuous monitoring of oscillatory and non-oscillatory tree movements under wind loading has been conducted in previous studies using clinometers and accelerometers [33,34].

Static and dynamic evaluation offer different but complementary perspectives, and their combined use can improve early detection of reduced stability. High-precision instruments (e.g., professional inclinometers or elasto-inclinometers) provide reliable data for quantitative biomechanical diagnosis of static tilt and root–soil anchorage; however, due to cost and logistics, they are usually reserved for high-value trees or post-event quantitative biomechanical assessment. As a result, there is still a lack of scalable, cost-effective solutions for long-term anchorage assessment in urban settings [21]. In this context, it is crucial to develop innovative approaches that can be applied on a large scale, particularly those capable of continuously acquiring data. Such solutions would enable real-time monitoring, facilitate proactive management, and support more effective decision making in urban forestry.

A recent study by Incollu et al. [35] demonstrated the potential of low-cost MEMS (Micro-Electro-Mechanical Systems) accelerometers for analyzing tree stability and monitoring dynamic responses. Laboratory tests showed that MEMS measurements were consistent with reference high-precision seismic sensors in detecting the dynamic response of a simple system under controlled conditions, including the identification of natural frequencies and initial oscillatory behavior. However, the study also revealed limitations in damping estimation as motion decayed, due to reduced oscillation amplitude and increased noise, highlighting the impact of sensor quality on measurement reliability. This underscores the need to carefully evaluate the practical applicability of MEMS sensors beyond

laboratory settings. Several studies confirm the effectiveness of MEMS for characterizing the dynamic response of trees [34,36,37]. Recent research has emphasized the increasing relevance of tree stability and risk assessment in urban forestry contexts [38–40]. Despite these advances, their use in safety-critical applications remains limited by key challenges such as metrological performance, repeatability, temperature sensitivity, and long-term drift under operational conditions [35].

Building on these findings, this study expands the experimental assessment of low-cost MEMS technologies by focusing on inclinometers and their suitability for static stability assessment. A comprehensive metrological evaluation was conducted, spanning controlled laboratory calibration to replicated in situ applications. The aim is to determine whether this technology can deliver reliable and accurate static stability information, including the ability to detect variations in inclination consistent with those measured by a professional high-precision inclinometer, and to assess its potential for scalable long-term deployment in urban tree risk management. Specifically, this study aims to:

(i) Quantify the performance of a low-cost MEMS inclinometer under controlled laboratory conditions using a geometric inclination reference;
(ii) Assess its stability and repeatability for quasi-static inclination measurements in replicated in situ pulling tests;
(iii) Discuss the implications of the experimental results in terms of potential scalability and future applications under typical urban operational constraints.

2. Materials and Methods

2.1. Experimental Design

To compare the performance of the inclinometer sensors, a two-phase evaluation was carried out, consisting of (i) controlled laboratory tests and (ii) field tests on standing trees under realistic conditions. A summary of the laboratory and field tests is provided in Table 1.

Table 1. Summary of the experimental tests. In the laboratory tests, the Stepcolumn lists the averaging window (seconds) associated with ID A–F. In the field tests, the Peak force (N) column reports the peak forces applied during the three pull-hold phases (1–3). Within each field test, the forces at 1.30 m and 2.70 m are identical because the same pulling protocol is used.

Category	Test Description	ID	Step	Peak Force (N)
Laboratory tests	LAB-1: Static tilt calibration with Borletti steel shims (0–20 mm), MEMS acquisition, various averaging windows (1–120 s).	A	1 s	–
		B	10 s	–
		C	30 s	–
		D	60 s	–
		E	90 s	–
		F	120 s	–
Field tests	FIELD-A:Controlled pulling test on a standing tree with sensors installed at 1.30 m and 2.70 m (reference high-precision inclinometer + MEMS co-located).	A	1	450
		A	2	917
		A	3	928
	FIELD-B: Controlled pulling test on a same standing tree with sensors installed at 1.30 m and 2.70 m (reference high-precision inclinometer + MEMS co-located).	B	1	843
		B	2	1002
		B	3	1017

2.2. Laboratory Tests

The laboratory test (LAB-1) was conducted using the low-cost MEMS inclinometer, a wireless prototype instrument featuring an STMicroelectronics MEMS triaxial chip. It offers a configurable full-scale acceleration range of $\pm 19.6\,\mathrm{m\,s^{-2}}$ and a sampling frequency of 26 Hz. The device operates via Wi-Fi transmission and can be powered by battery or continuous supply; in this study, battery mode was used.

The inclination was assessed on a cantilever steel beam with a rectangular cross-section of 50 mm × 5 mm and length $L = 2000$ mm. The MEMS sensor was mounted on the upper surface of the beam and secured with nylon ties (Figure 1a). Calibrated Borletti steel gauge blocks were progressively inserted beneath the free end to impose a controlled tilt angle, with shim thickness h^* increased stepwise from 1 to 20 mm.

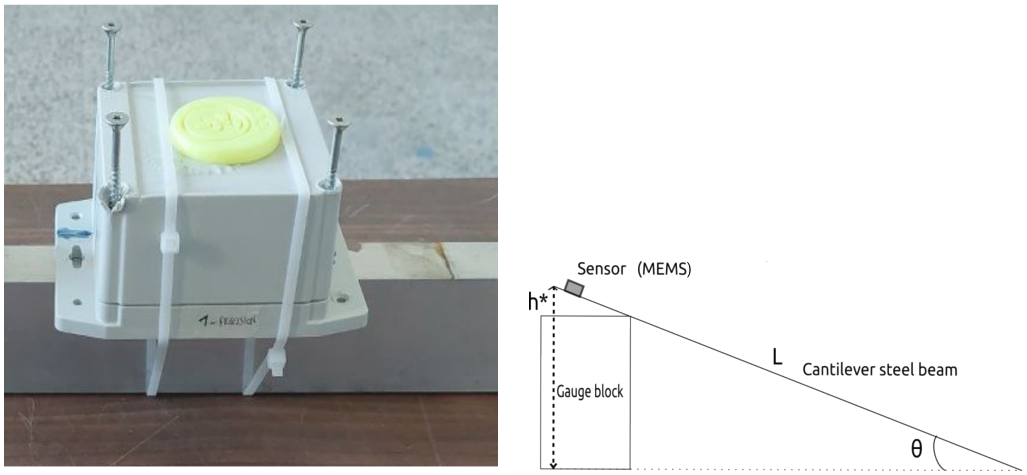


Figure 1. Laboratory tests: (**a**) low-cost MEMS inclinometer mounted on the steel beam during the controlled tilting experiment; (**b**) schematic relation between shim thickness h^*, horizontal projection L, and inclination angle θ.

The expected inclination angle of the setup geometry is:

$$\theta_{\mathrm{exp}} = \arcsin\left(\frac{h^*}{L}\right), \tag{1}$$

For $L = 2000$ mm, this yields $\theta_{\mathrm{exp}} = 0.0286°$ for $h^* = 1$ mm and $\theta_{\mathrm{exp}} = 0.5729°$ for $h^* = 20$ mm.

The MEMS data (a_x, a_y, a_z) were converted to inclination (degrees) via the two-argument arctangent function. The function $\mathrm{atan2}(y, x)$ provides correct quadrant determination from the signs of its inputs and avoids divisions by zero, whereas $\arctan(y/x)$ loses quadrant information and becomes numerically unstable when $x \approx 0$. Being continuous over $(-\pi, \pi]$, atan2 was used to compute inclination as

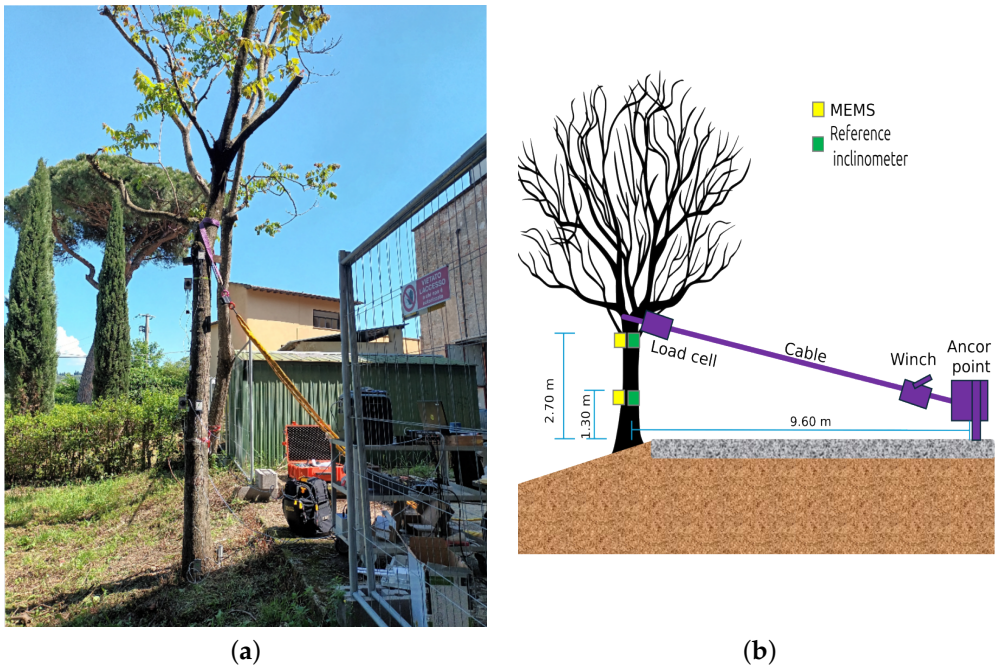
$$\theta = \mathrm{atan2}\left(a_x, \sqrt{a_y^2 + a_z^2}\right) \cdot \frac{180}{\pi}, \tag{2}$$

Angle estimates were then averaged using the windows specified in Section 2.4 (1–120 s).

2.3. Field Tests

Field experiments were carried out on a recently pruned *Ailanthus altissima* Mill (Tree of Heaven), located within the Department of Civil and Environmental Engineering of the University of Florence Figure 2a). The selected tree, previously used as a test tree for the

study by Incollu et al. [35], served as a reference for evaluating the in situ performance of the sensors. The main characteristics of the tree are reported in Table 2.



(**a**) (**b**)

Figure 2. Field tests: (**a**) field test setup (photograph of the tree during testing); (**b**) schematic of the pulling-test configuration, with MEMS sensors and reference high-precision inclinometers installed at 1.30 m and 2.70 m on the stem, load cell at the cable attachment point, and winch anchored at a distance of 9.60 m.

Table 2. Characteristics of the investigated tree and measurement methods.

Parameter	Value	Acquisition Method
Diameter at breast height (DBH)	17.5 cm	Caliper
Total height	11 m	Vertex hypsometer
Crown area	5 m^2	Manual delineation on orthophoto

The reference instrument used in the field was a Dynatim™ biaxial high-precision inclinometer (RINNTECH, Heidelberg, Germany). This instrument is widely recognized in professional tree-pulling systems for assessing tree stability under static loading. In this study, this instrument is referred to as the reference high-precision inclinometer and was used exclusively for the field comparisons. It features a measurement range of ±15° and a nominal resolution of 0.001°, allowing continuous recording of tilt under static or dynamic loading. The sensor operates via a cabled connection to a computer-based acquisition unit with dedicated software for real-time recording and data storage. In this study, the reference inclinometer was used exclusively for the field comparisons (Figure 3).

The site was characterized by sloping terrain with an average inclination of about 20%. The root system was embedded in natural soil on the side opposite the pulling direction, while in the pulling direction, the root system extended beneath a compacted industrial surface. These conditions resemble those often encountered in urban roadside environments.

A load cell installed in line with the pulling cable, at approximately 3 m above ground, continuously recorded the pulling force. The pulling point on the stem was located at a horizontal distance of about 9.60 m from the anchoring system.



Figure 3. Co-located installation of the low-cost MEMS inclinometer (right) and the reference high-precision inclinometer (left) during the field tests.

Two MEMS sensors were installed at heights of 1.30 m (DBH, commonly used as the reference level) and 2.70 m, each co-located with a reference high-precision inclinometer. This two-height arrangement was chosen to (i) assess whether sensor elevation along the stem influences the agreement and reliability of static tilt estimates and (ii) emulate a practical mounting height for urban deployments. The 2.70 m position was selected to reduce the likelihood of accidental contact (e.g., by pedestrians or vehicles) and vandalism while remaining accessible for battery replacement and routine maintenance. However, it should be noted that these heights deviate from the standard Static Integrated Method (SIM) protocol, which requires placing inclinometers at the root collar to isolate root-plate rotation and compare it against established safety thresholds (e.g., 0.25°). In this study, sensors were installed at 1.30 m and 2.70 m to prioritize metrological characterization, because the larger inclination amplitudes at these positions enable a more robust instrument-to-instrument comparison than the very small rotations typically recorded at the root collar. At these heights, the measured inclination reflects the combined contribution of root-plate rotation and stem bending; therefore, the present results are not directly comparable with SIM basal-rotation thresholds and do not provide SIM-compliant anchorage classification. Controlled pulling tests were performed along the longitudinal axis of the tree. The stem was gradually loaded in tension, held in a static deflected position for three minutes, then further tensioned and held again for three minutes. This cycle was repeated three times, followed by a controlled release of the pulling line. The peak forces applied in the three pull–hold phases of Tests A–B are summarized in Table 1. Note that, within each test, force levels were identical at 1.30 m and 2.70 m due to the same pulling protocol. Cable angle effects ($\theta \approx 15$–20° from terrain slope) on lateral force were accounted for in protocol design ($F_{\text{lateral}} = F_{\text{measured}} \times \cos\theta$), with peaks maintained below 10% DBH-equivalent thresholds for safety; however, decomposition was omitted from analysis, as co-located sensors experienced identical moments under shared loading [31].

2.4. Data Processing

An internal data-processing protocol was designed to ensure full comparability and reproducibility between the laboratory and field datasets. Although the physical conditions differ (controlled tilt versus in situ pulling), both workflows share a common analytical structure comprising: (i) preliminary inspection and quality control, (ii) trigonometric conversion of accelerometric data to inclination, (iii) signal pre-processing and

despiking, (iv) averaging and filtering procedures adapted to each context, (v) baseline or reference-level definition, and (vi) computation of error or agreement metrics (Figure 4). Synchronization between instruments was required only for the field measurements.

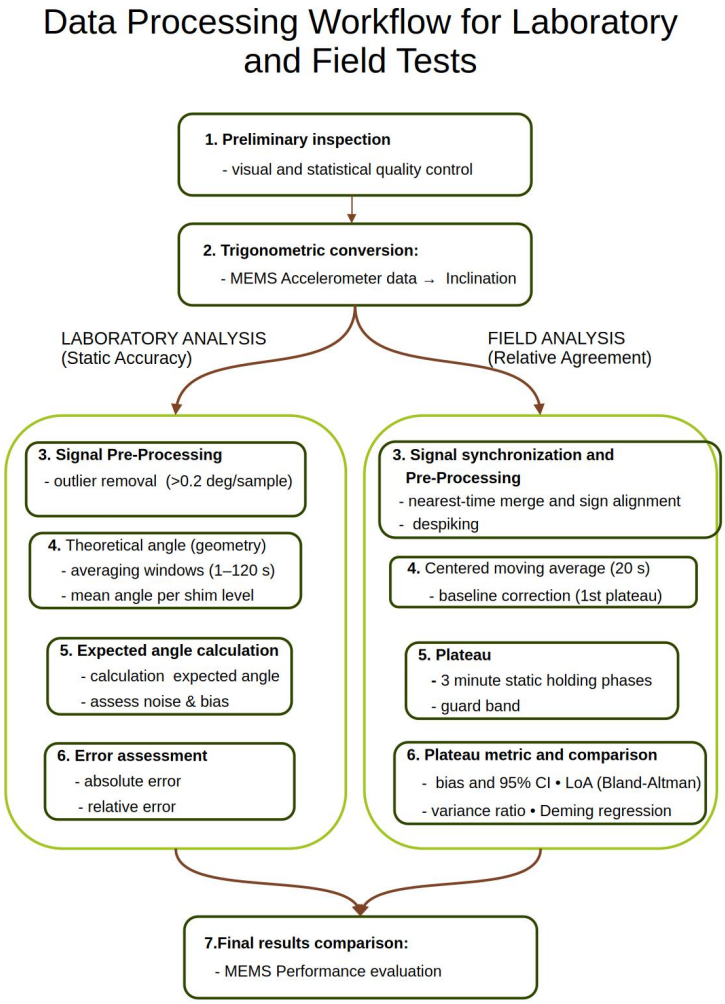


Figure 4. Data processing workflow for the laboratory (left) and field (right) phases. The two workflows share common preprocessing elements (inspection, trigonometric conversion, despiking, and metric computation) but differ in focus: laboratory analysis quantifies absolute metrological accuracy under controlled static conditions, whereas field analysis additionally requires synchronization between instruments and emphasizes quasi-static filtering, baseline correction, and agreement modelling using Bland–Altman and Deming regression.

2.4.1. Laboratory Data

Laboratory processing focused on the absolute metrological performance of the MEMS inclinometer under fully static conditions. After visual inspection, MEMS signals were aligned on a shared internal time base and converted trigonometrically into inclination (θ) using the sensor geometry. A set of averaging windows (1–120 s) was applied to assess how temporal averaging affects random noise and bias. For each static step, the theoretical inclination was computed from the beam geometry, and errors were obtained as

$$\Delta x_{\mathrm{abs}} = x_{\mathrm{ref}} - x_{\mathrm{meas}}, \tag{3}$$

$$\Delta x_{\mathrm{rel}} = \frac{\Delta x_{\mathrm{abs}}}{x_{\mathrm{ref}}} \times 100, \tag{4}$$

where

- x_{ref} is the theoretical (expected) inclination θ_{exp} derived from the geometric configuration of the beam;
- x_{meas} is the inclination measured by the MEMS sensor;
- Δx_{abs} is the absolute error, computed as $x_{ref} - x_{meas}$, expressed in degrees [°];
- Δx_{rel} is the relative error, defined as the ratio between the absolute error and the corresponding expected value x_{ref} (dimensionless).

2.4.2. Field Data

Field measurements introduced small dynamic components (e.g., residual stem sway, elastic relaxation, minor force adjustments), requiring additional processing to isolate quasi-static inclinations. Each plateau represented a 3-min static holding phase during which a constant pulling load was maintained. The workflow included the following steps:

1. **Preliminary inspection:** Visual and statistical screening of raw time series to ensure signal integrity and identify missing data or sensor drift.
2. **Signal synchronization:** Reference high-precision inclinometer timestamps were reconstructed as $t_{Ref} = t_0 + t_{ms}$, while MEMS timestamps were absolute. A nearest-time merge was therefore sufficient to align both datasets, precluding the need for drift correction. The reference axis was a reference high-precision inclinometer X, sign-aligned to MEMS.
3. **Trigonometric conversion:** Accelerometric data were converted into inclination angles consistent with the laboratory reference frame.
4. **Pre-processing:** Based on laboratory findings, where longer averaging windows systematically reduced random noise without altering the mean inclination, a centered 20 s moving average was adopted for field data to stabilize plateau estimates during the 3-min holds, attenuating high-frequency noise while preserving the step-like transitions between successive pull–hold phases (26 Hz $\approx$ 520 samples). This window length represents an operational compromise derived from laboratory calibration results and tailored to the duration of the field holding phases.
5. **Relative baseline:** The first stable plateau was used as reference. Each series was centered by subtracting its median value over this window, i.e., $\mathrm{Ref} - \mathrm{median}(\mathrm{Ref})$ and $\mathrm{MEMS} - \mathrm{median}(\mathrm{MEMS})$, thereby removing absolute offset differences.
6. **Plateau metrics and statistical comparison:** Bland–Altman analysis [41] was used to evaluate systematic bias and limits of agreement (LoA) between the two instruments, providing a direct visualization of measurement consistency across the amplitude range. Deming regression [42,43] was applied to model the linear relationship between MEMS and the reference high-precision inclinometer, accounting for uncertainty in both variables.

Each plateau was analyzed on its central portion, excluding a $\pm$12 s guard band to remove transient oscillations and moving-average edge effects. This interval was empirically determined as the time required for both sensors to stabilize after each load change.

Overall, the analytical pipeline (Figure 4) integrates reproducible steps from raw signal alignment to final agreement metrics, ensuring that comparisons between MEMS and reference high-precision inclinometers remain both statistically valid and physically interpretable across experimental conditions.

3. Results

3.1. Laboratory Test

The laboratory calibration compares the tilt expected from the setup geometry (gauge block thickness and beam length) to the inclination derived from MEMS signals. Across the

six averaging windows (represented in Figure 5a–f), the expected measured curves show a progressive reduction in scatter as the window length increases.

Short windows (Figure 5a–c, 1–30 s) exhibit noisier estimates and larger deviations at small imposed tilts, whereas windows ≥60 s (Figure 5d–f) yield trajectories that closely follow the theoretical trend. This behaviour is consistent over the full shim range (up to 20 mm).

Table 3 summarizes the MEMS performance by shim thickness for the 120 s averaging window (corresponding to Figure 5f). Absolute errors remain on the order of a few hundredths of a degree over the full angular range. At small imposed tilts (1–3 mm), relative errors are largest by construction, with values on the order of 15%–20%. As the angle increases, relative errors decrease, remaining mostly below approximately 7% in the 5–10 mm range and dropping to 0.9% at 20 mm (Table 3). These results confirm that, under static conditions and with adequate averaging, the MEMS inclinometer closely reproduces the expected geometric inclination, with performance degradation occurring primarily at the smallest angles.

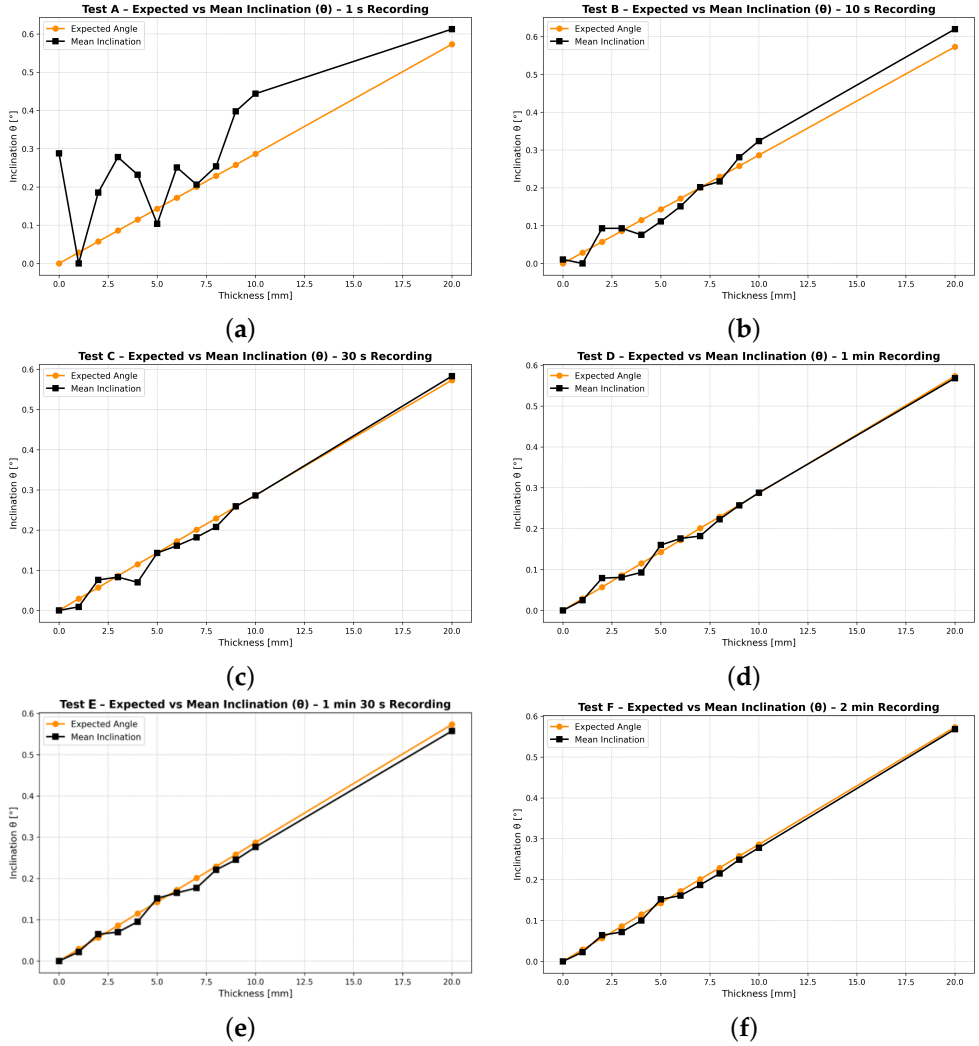


Figure 5. Laboratory calibration results comparing MEMS measurements with theoretical geometric inclination across different averaging windows: (**a**) 1 s, (**b**) 10 s, (**c**) 30 s, (**d**) 60 s, (**e**) 90 s, and (**f**) 120 s. The progressive reduction in noise and stabilization of the signal is visible as the window length increases.

Table 3. Laboratory calibration (Test F, 120 s averaging window). Expected inclination from beam geometry (x_{ref}) and MEMS-measured angles, with corresponding absolute and relative errors.

Thickness [mm]	x_{ref} [°]	MEMS Measured [°]	Δx_{abs} [°]	Δx_{rel} [%]
0	0.000	0.000	0.000	–
1	0.029	0.023	0.006	20.7
2	0.057	0.066	−0.009	−15.2
3	0.086	0.073	0.013	15.0
4	0.115	0.100	0.015	12.7
5	0.143	0.153	−0.010	−6.8
6	0.172	0.163	0.009	5.2
7	0.201	0.187	0.014	6.7
8	0.229	0.216	0.013	5.8
9	0.258	0.251	0.007	2.6
10	0.286	0.279	0.007	2.6
20	0.573	0.568	0.005	0.9

3.2. Field Test

All field comparisons were conducted in the relative domain along the longitudinal direction aligned with the *X*-axis of the reference high-precision inclinometer. Test A and Test B were performed on the same tree and experimental setup and included co-located MEMS and reference high-precision inclinometers; together, they represent pulling sessions carried out under different (increasing) load levels, used to assess the stability and robustness of the instrument-to-instrument agreement across loading conditions. In all configurations, the reference high-precision inclinometer was co-located with the MEMS sensor to provide a continuous reference baseline for agreement assessment. For each test and height, Figure 6 shows the relative time histories, while Figure 7 presents the corresponding agreement scatter with Deming regression.

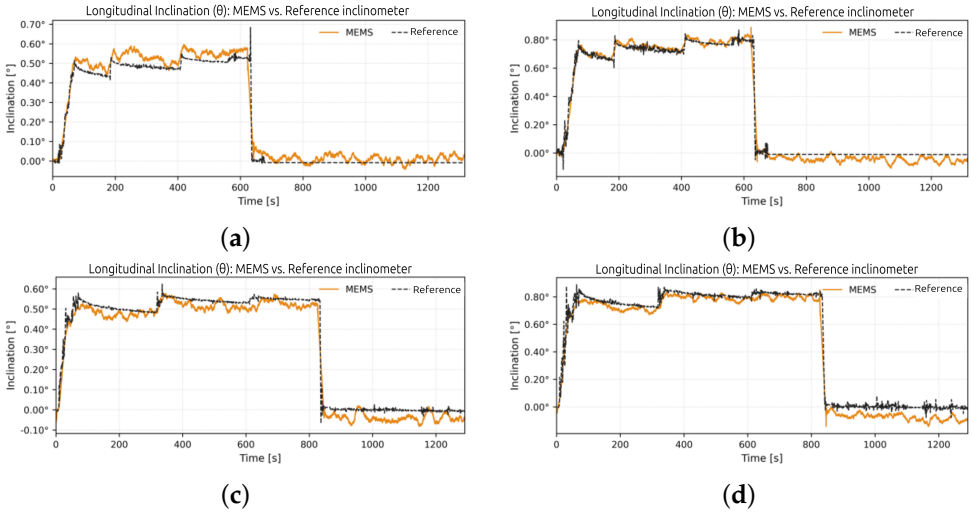


Figure 6. Relative inclination time histories after baseline subtraction: (**a**) Test A at 1.30 m; (**b**) Test A at 2.70 m; (**c**) Test B at 1.30 m; (**d**) Test B at 2.70 m.

In Test A at 1.30 m, the relative time series show consistent co-variation (Figure 6a). The agreement plot (Figure 7a) shows data points clustering near the identity line; the Deming fit yields $a = +0.020°$, $b = 1.038$. Similarly, Test A at 2.70 m (Figures 6b and 7b) confirms this high concordance. In Test B, the results at 1.30 m (Figures 6c and 7c) and 2.70 m (Figures 6d and 7d) confirm the stability of the MEMS prototype across repeated trials. Detailed statistics for all tests are summarized in Table 4.

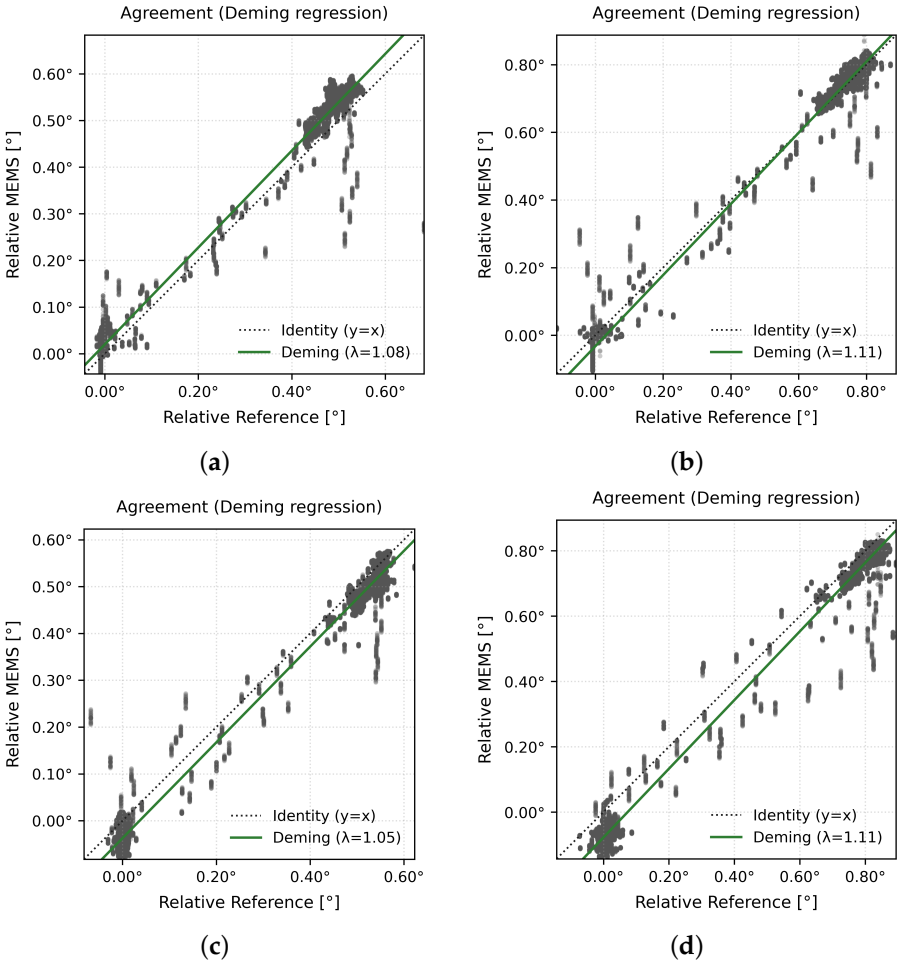


Figure 7. Agreement scatter with identity line ($y = x$) and Deming regression: (**a**) Test A at 1.30 m; (**b**) Test A at 2.70 m; (**c**) Test B at 1.30 m; (**d**) Test B at 2.70 m.

Across Tests A–B and both heights, the correlation coefficients remain very high ($r = 0.993$–0.996) with small RMSE $\approx 0.04°$–$0.07°$. Detailed statistics are summarized in Table 4.

Table 4. Summary of agreement metrics by test and sensor height. Deming regression is reported as MEMS $= a + b \times$ Ref, where Ref denotes the reference high-precision inclinometer. Bland–Altman reports bias and limits of agreement (LoA) at the mean of measurements. All angular quantities are expressed in degrees.

Test (Height)	N_{samp}	r	RMSE (°)	a (°)	b	λ	BA Bias (°)	BA LoA (°)
Test A (1.30 m)	33,888	0.993	0.042	0.020	1.038	1.08	0.028	[−0.014, 0.070]
Test A (2.70 m)	35,978	0.996	0.041	−0.033	1.052	1.11	−0.015	[−0.065, 0.034]
Test B (1.30 m)	33,226	0.995	0.040	−0.037	1.023	1.05	−0.030	[−0.072, 0.012]
Test B (2.70 m)	35,258	0.996	0.065	−0.078	1.052	1.11	−0.051	[−0.103, 0.001]

4. Discussion

The present study assessed the metrological reliability of a low-cost MEMS inclinometer under both controlled laboratory and field conditions. By combining laboratory calibration with in situ validation, it provides an evaluation of the instrument's performance across different levels of environmental control and signal stability, explicitly distinguishing between sensor metrological performance and the mechanical response of the tree–soil system under load.

Laboratory calibration offered a controlled framework to evaluate how temporal averaging influences the accuracy of MEMS-based inclination estimates relative to a geometric reference. Figures 5 and Table 3 show a progressive stabilization of the MEMS signal as the averaging window increases. Short windows (1–30 s) result in noisier estimates and larger deviations at small imposed tilts, whereas windows ≥60–120 s yield inclination curves that closely track the theoretical trend across the considered angle range. At a 120 s window, absolute errors remain on the order of a few hundredths of a degree, while relative errors are largest at the smallest angles and decrease with increasing tilt amplitude. Overall, these results illustrate the expected trade-off between temporal responsiveness and noise suppression in MEMS-based inclination measurements and are consistent with previous evidence on the role of filtering and signal amplitude in MEMS accuracy [34,36]. The laboratory outcomes also informed the design of the field data-processing strategy.

Field analyses were conducted in the relative domain, after baseline subtraction on the first stable plateau, and focused on the longitudinal component co-aligned with the reference high-precision inclinometer. Across both tests (A and B) and both installation heights (1.30 m and 2.70 m), the paired time histories exhibit step-like responses during loading and holding phases, with synchronous reversals upon load release. Agreement analyses show clustering around the identity line, with Deming slopes close to unity, small intercepts, and narrow Bland–Altman limits of agreement. The pooled indicators reported in Table 4 confirm consistently high agreement between the MEMS sensor and the reference instrument, with low dispersion across configurations. These patterns are in line with established practice, the comparative assessment and characterization of low-cost inertial sensors in tree biomechanics, where agreement is evaluated through time-domain co-variation and error-in-variables regression [33,34,37].

During the constant-load phases of the pulling tests, both sensors recorded a gradual decrease in inclination despite constant applied force. The synchronous occurrence of this trend in the MEMS and reference signals suggests that it reflects a physical response of the stem–root–soil system rather than instrumental drift. This behaviour is consistent with time-dependent mechanical relaxation or hysteretic effects under sustained bending, as reported in previous biomechanical studies [23,44,45]. From a metrological perspective, this observation indicates that the MEMS sensor is capable of resolving subtle, short-term inclination variations under quasi-static loading conditions.

The two experimental phases address complementary objectives. Laboratory tests quantify absolute agreement with a theoretical reference under fully controlled conditions, whereas field tests assess relative agreement against a professional inclinometer during pull–and–hold sequences. Because sensors were mounted at 1.30 m and 2.70 m, the measured inclination integrates both stem bending and root-plate rotation and therefore does not provide SIM-compliant basal rotation or anchorage classification. Instead, the field results demonstrate the consistency of quasi-static inclination measurements above the root collar, where signal amplitudes are sufficient for robust instrument-to-instrument comparison.

From an operational standpoint, the laboratory and field results identify the conditions under which MEMS sensors yield the most stable inclination estimates, namely, the use of sufficiently long averaging windows and a well-defined baseline. Under these conditions, the MEMS prototype reliably tracks the longitudinal inclination component measured by the reference instrument during controlled pulling tests. The low cost, battery-powered wireless operation, and ease of deployment of MEMS devices make them suitable for repeated or multi-point quasi-static assessments that are often impractical with professional high-precision inclinometers. Broader application would benefit from standardized procedures for windowing, baseline definition, and sensor alignment, as well as replication

across species and site conditions to characterize variability related to mounting and local dynamics [34].

Field comparisons were restricted to relative measurements along a single axis, and absolute inclination accuracy under field conditions was not addressed. Small-angle behaviour in the laboratory shows higher relative error by construction, and long-term effects such as thermal drift and sensor ageing remain outside the scope of this study. These limitations are typical of MEMS characterization studies and motivate future investigations aimed at extending the operational envelope of low-cost inclination sensing in arboricultural applications [34,36].

5. Conclusions

This study provides a preliminary metrological characterization of a low-cost MEMS inclinometer for tree stability assessment by combining laboratory calibration against a geometric reference with field benchmarking using a high-precision, biaxial reference inclinometer.

In controlled tilting tests, longer averaging windows ($\geq$60–120 s) substantially reduced measurement scatter and improved adherence to the theoretical inclination across the full angular range; at 120 s, absolute errors were limited to a few hundredths of a degree (MEMS $\approx$ 0.005–0.015°), with larger relative deviations only at the smallest tilts.

Field applications confirmed the reproducibility of quasi-static inclinations and the ability of the MEMS device to detect small, time-dependent variations under constant-load phases, consistent with mechanical relaxation of the stem–root system and soil–root interface deformation. Overall, the MEMS inclinometer demonstrated sufficient accuracy, temporal stability, and sensitivity to capture subtle static tilt variations during field deployments.

Beyond the metrological characterization, the deployment of multiple sensors along the stem explored in this study, through measurements at two different heights, suggests a promising perspective for analyzing stem deformation patterns and constructing bending curves. Such applications could provide valuable insights into localized structural integrity and strain distribution, which are currently difficult to implement on a large scale with professional equipment due to cost and logistical constraints.

Future work should verify the long-term stability and thermal behaviour of the instrument under extended in situ operation, and broaden testing across multiple trees, species, and site conditions to assess scalability, inter-tree variability, and overall operational robustness.

Author Contributions: Conceptualization, Y.G., F.G. (Francesca Giannetti), A.G., G.B. and I.I.; methodology: I.I., Y.G., A.G. and H.A.C.; software: H.A.C. and I.I.; formal analysis: I.I., Y.G., A.G. and H.A.C.; resources: Y.G., F.G. (Francesca Giannetti), G.B. and F.G. (Filippo Giadrossich); data curation: I.I., Y.G., A.G. and H.A.C.; writing—original draft preparation: I.I., Y.G. and F.G. (Francesca Giannetti); writing—review and editing: I.I., Y.G., F.G. (Francesca Giannetti), G.B., A.G., H.A.C., F.G. (Filippo Giadrossich) and T.T.; supervision: Y.G., F.G. (Francesca Giannetti) and F.G. (Filippo Giadrossich). All authors have read and agreed to the published version of the manuscript.

Funding: This research was carried out as part of the PhD course in Agricultural Sciences at the University of Sassari (XXXVIII cycle), supported by a scholarship co-funded by Ministerial Decree No. 352 of 9 April 2022, under the National Recovery and Resilience Plan (PNRR)—funded by the European Union—NextGenerationEU, Mission 4 "Education and Research", Component 2 "From Research to Enterprise", Investment 3.3, and by Bluebiloba Startup Innovativa S.r.l. and Elighes S.r.l. For the authors Francesca Giannetti, Gianni Bartoli, Andrea Giachetti, Ilaria Incollu, Tommaso Tognetti, and Yamuna Giambastiani, this work was funded by the European Union under the Horizon Europe Programme–HORIZON-RIA (Research and Innovation Actions), Call "Disaster-Resilient

Society 2024" (HORIZON-CL3-2024-DRS-01), through grant agreement No. 101225988, project *TREESURE-Decision support Tool for Risk Evaluation, management and awareness of tree Failure Disasters.*

Data Availability Statement: The data are not publicly available due to privacy or confidentiality restrictions.

Acknowledgments: The authors would like to thank Vincenzo Barillà and Lorenzo Massai for their valuable assistance in assembling and testing the prototype. Their contribution was essential to the initiation of this work.

Conflicts of Interest: The authors declare no conflicts of interest.

References

1. Bottalico, F.; Travaglini, D.; Chirici, G.; Garfì, V.; Giannetti, F.; Marco, A.D.; Fares, S.; Marchetti, M.; Nocentini, S.; Paoletti, E.; et al. A spatially-explicit method to assess the dry deposition of air pollution by urban forests in the city of Florence, Italy. *Urban For. Urban Green.* **2017**, *27*, 221–234. https://doi.org/10.1016/J.UFUG.2017.08.013.
2. Haase, D.; Larondelle, N.; Andersson, E.; Artmann, M.; Borgström, S.; Breuste, J.; Gomez-Baggethun, E.; Gren, Å; Hamstead, Z.; Hansen, R.; et al. A quantitative review of urban ecosystem service assessments: Concepts, models, and implementation. *Ambio* **2014**, *43*, 413–433. https://doi.org/10.1007/S13280-014-0504-0.
3. Ariluoma, M.; Ottelin, J.; Hautamäki, R.; Tuhkanen, E.M.; Mänttäri, M. Carbon sequestration and storage potential of urban green in residential yards: A case study from Helsinki. *Urban For. Urban Green.* **2021**, *57*, 126939. https://doi.org/10.1016/J.UFUG.2020.126939.
4. Gómez-Baggethun, E.; Barton, D.N. Classifying and valuing ecosystem services for urban planning. *Ecol. Econ.* **2013**, *86*, 235–245. https://doi.org/10.1016/J.ECOLECON.2012.08.019.
5. Meili, N.; Manoli, G.; Burlando, P.; Carmeliet, J.; Chow, W.T.; Coutts, A.M.; Roth, M.; Velasco, E.; Vivoni, E.R.; Fatichi, S. Tree effects on urban microclimate: Diurnal, seasonal, and climatic temperature differences explained by separating radiation, evapotranspiration, and roughness effects. *Urban For. Urban Green.* **2021**, *58*, 126970. https://doi.org/10.1016/J.UFUG.2020.126970.
6. Bolund, P.; Hunhammar, S. Ecosystem services in urban areas. *Ecol. Econ.* **1999**, *29*, 293–301. https://doi.org/10.1016/S0921-8009(99)00013-0.
7. Akubue, J.A. Effects of Street Geometry on Airflow Regimes for Natural Ventilation in Three Different Street Configurations in Enugu City. In *Different Strategies of Housing Design*; Çakmaklı, A.B., Ed.; IntechOpen: London, UK, 2019; Chapter 2. https://doi.org/10.5772/intechopen.84786.
8. Biao, L.; Cunyan, J.; Lu, W.; Weihua, C.; Jing, L. A parametric study of the effect of building layout on wind flow over an urban area. *Build. Environ.* **2019**, *160*, 106160. https://doi.org/10.1016/j.buildenv.2019.106160.
9. Cui, D.; Li, X.; Liu, J.; Yuan, L.; Mak, C.; Fan, Y.; Kwok, K. Effects of building layouts and envelope features on wind flow and pollutant exposure in height-asymmetric street canyons. *Build. Environ.* **2021**, *205*, 108177. https://doi.org/10.1016/j.buildenv.2021.108177.
10. Mullaney, J.; Lucke, T.; Trueman, S.J. A review of benefits and challenges in growing street trees in paved urban environments. *Landsc. Urban Plan.* **2015**, *134*, 157–166. https://doi.org/10.1016/J.LANDURBPLAN.2014.10.013.
11. Döhren, P.V.; Haase, D. Ecosystem disservices research: A review of the state of the art with a focus on cities. *Ecol. Indic.* **2015**, *52*, 490–497. https://doi.org/10.1016/J.ECOLIND.2014.12.027.
12. Buson, M.; Bortolini, L. Analysis of Tree Falls Caused by Weather Events in Urban Areas: The Case Study of the City of Venice. *Land* **2025**, *14*, 1131. https://doi.org/10.3390/land14061131.
13. Van Haaften, M.; Gardebroek, C.; Heijman, W.; Meuwissen, M.M. Injuries and deaths due to tree failure in The Netherlands: Analysis of observational data from 1998–2021. *Sci. Rep.* **2024**, *14*, 22415. https://doi.org/10.1038/s41598-024-73716-x.
14. Schmidlin, T.W. Human fatalities from wind-related tree failures in the United States, 1995–2007. *Nat. Hazards* **2009**, *50*, 13–25. https://doi.org/10.1007/s11069-008-9314-7.
15. Koeser, A.K.; Hauer, R.J.; Miesbauer, J.W.; Peterson, W. Municipal tree risk assessment in the United States: Findings from a comprehensive survey of urban forest management. *Arboric. J.* **2016**, *38*, 218–229. https://doi.org/10.1080/03071375.2016.1221178.
16. Portoghesi, L.; Masini, E.; Tomao, A.; Agrimi, M. Could climate change and urban growth make Europeans regard urban trees as an additional source of danger? *Front. For. Glob. Chang.* **2023**, *6*, 1155016. https://doi.org/10.3389/FFGC.2023.1155016.
17. Roman, L.A.; Conway, T.M.; Eisenman, T.S.; Koeser, A.K.; Barona, C.O.; Locke, D.H.; Jenerette, G.D.; Östberg, J.; Vogt, J. Beyond 'trees are good': Disservices, management costs, and tradeoffs in urban forestry. *Ambio* **2021**, *50*, 615–630. https://doi.org/10.1007/S13280-020-01396-8.

18. Ordóñez, C.; Threlfall, C.G.; Livesley, S.J.; Kendal, D.; Fuller, R.A.; Davern, M.; van der Ree, R.; Hochuli, D.F. Decision-making of municipal urban forest managers through the lens of governance. *Environ. Sci. Policy* **2020**, *104*, 136–147. https://doi.org/10.1016/J.ENVSCI.2019.11.008.
19. Linhares, C.S.; Gonçalves, R.; Martins, L.M.; Knapic, S. Structural stability of urban trees using visual and instrumental techniques: A review. *Forests* **2021**, *12*, 1752. https://doi.org/10.3390/f12121752.
20. Mattheck, C.; Breloer, H. Field guide for visual tree assessment (VTA). *ARboricultural J.* **1994**, *18*, 1–23. https://doi.org/10.1080/03071375.1994.9746995.
21. Allison, R.B.; Wang, X.; Senalik, C.A. Methods for Nondestructive Testing of Urban Trees. *Forests* **2020**, *11*, 1341. https://doi.org/10.3390/f11121341.
22. Wessolly, L.; Erb, M. *Handbuch der Baumstatik und Baumkontrolle*; Patzer Verlag: Berlin, Germany, 1998.
23. Lundström, T.; Jonas, T.; Stöckli, V.; Ammann, W. Anchorage of mature conifers: Resistive turning moment, root–soil plate geometry and root growth orientation. *Tree Physiol.* **2007**, *27*, 1217–1227. https://doi.org/10.1093/treephys/27.9.1217.
24. James, K.R.; Dahle, G.A.; Grabosky, J.; Kane, B.; Detter, A. Tree biomechanics literature review: Dynamics. *Arboric. Urban For.* **2014**, *40*, 1–15. https://doi.org/10.48044/JAUF.2014.001.
25. Wessolly, L. Stability of Trees: Explanation of the Tipping Process. *Stadt und Grün* **1996**, *4*, 268–272.
26. Jonsson, M.J.; Foetzki, A.; Kalberer, M.; Lundström, T.; Ammann, W.; Stöckli, V. Root–soil rotation stiffness of Norway spruce (*Picea abies* (L.) Karst) growing on subalpine forested slopes. *Plant Soil* **2006**, *285*, 267–277. https://doi.org/10.1007/s11104-006-9013-7.
27. Esche, D.; Schumacher, P.; Detter, A.; Rust, S. Experimentelle Überprüfung der Windlastanalyse für statische Zugversuche. In *Jahrbuch der Baumpflege*; Dujesiefken, D., Ed.; Haymarket Media: Augsburg, Germany, 2018; pp. 229–236.
28. Giambastiani, Y.; Preti, F.; Errico, A.; Sani, L. On the Tree Stability: Pulling Tests and Modelling to Assess the Root Anchorage. *Procedia Environ. Sci. Eng. Manag.* **2017**, *4*, 237–244..
29. Detter, A.; Rust, S.; Böttcher, J.; Bouillon, J. Ambient Influences on the Results of Non-Destructive Pulling Tests. In *21st International Nondestructive Testing and Evaluation of Wood Symposium*; Wang, X., Sauter, U.H., Ross, R.J., Eds.; U.S. Department of Agriculture, Forest Service, Forest Products Laboratory: Madison, WI, USA, 2019; General Technical Report FPL-GTR-272; pp. 422–436.
30. Peterson, C.J.; Claassen, V. An evaluation of the stability of *Quercus lobata* and *Populus fremontii* on river levees assessed using static winching tests. *Forestry* **2013**, *86*, 201–209. https://doi.org/10.1093/forestry/cps079.
31. Detter, A.; Rust, S.; Krišāns, O. Experimental Test of Non-Destructive Methods to Assess the Anchorage of Trees. *Forests* **2023**, *14*, 533. https://doi.org/10.3390/F14030533.
32. Nicoll, B.C.; Gardiner, B.A.; Rayner, B.; Peace, A.J. Anchorage of coniferous trees in relation to species, soil type, and rooting depth. *Can. J. For. Res.* **2006**, *36*, 1871–1883. https://doi.org/10.1139/X06-072.
33. Schindler, D. Responses of Scots pine trees to dynamic wind loading. *Agric. For. Meteorol.* **2008**, *148*, 1733–1742. https://doi.org/10.1016/J.AGRFORMET.2008.06.003.
34. Kolbe, S.; Schindler, D. TreeMMoSys: A low cost sensor network to measure wind-induced tree response. *HardwareX* **2021**, *9*, e00180. https://doi.org/10.1016/J.OHX.2021.E00180.
35. Incollu, I.; Giachetti, A.; Giambastiani, Y.; Corti, H.A.; Giannetti, F.; Bartoli, G.; Piredda, I.; Giadrossich, F. Feasibility of a Low-Cost MEMS Accelerometer for Tree Dynamic Stability Analysis: A Comparative Study with Seismic Sensors. *Forests* **2025**, *16*, 1572. https://doi.org/10.3390/F16101572.
36. Yang, Z.; Hui, K.W.; Abbas, S.; Zhu, R.; Kwok, C.Y.T.; Heo, J.; Ju, S.; Wong, M.S. A Review of Dynamic Tree Behaviors: Measurement Methods on Tree Sway, Tree Tilt, and Root–Plate Movement. *Forests* **2021**, *12*, 379. https://doi.org/10.3390/F12030379.
37. Van Emmerik, T.; Steele-Dunne, S.; Hut, R.; Gentine, P.; Guerin, M.; Oliveira, R.S.; Wagner, J.; Selker, J.; Van De Giesen, N. Measuring tree properties and responses using low-cost accelerometers. *Sensors* **2017**, *17*, 1098. https://doi.org/10.3390/s17051098.
38. Herath, P.; Bai, X. Benefits and co-benefits of urban green infrastructure for sustainable cities: Six current and emerging themes. *Sustain. Sci.* **2024**, *19*, 1039–1063. https://doi.org/10.1007/S11625-024-01475-9.
39. Shiravi, M.; Depina, I.; Uzielli, M.; Bartoli, G. A Novel Methodology for Modeling the Effects of Geometrical Uncertainties in Tree Root-Soil Geometry on Tree Uprooting. *Biogeotechnics* 2025, *in press*. https://doi.org/10.1016/J.BGTECH.2025.100183.
40. Masini, E.; Tomao, A.; Corona, P.; Fattorini, L.; Giuliarelli, D.; Portoghesi, L.; Agrimi, M. The ecosystem disservices of trees on sidewalks: A study based on a municipality urban tree inventory in Central Italy. *Urban For. Urban Green.* **2023**, *86*, 128007. https://doi.org/10.1016/J.UFUG.2023.128007.
41. Bland, J.M.; Altman, D.G. Statistical Methods for Assessing Agreement Between Two Methods of Clinical Measurement. *Lancet* **1986**, *327*, 307–310. https://doi.org/10.1016/S0140-6736(86)90837-8.
42. Deming, W.E. *Statistical Adjustment of Data*; John Wiley & Sons: New York, NY, USA, 1943.
43. Linnet, K. Evaluation of Regression Procedures for Methods Comparison Studies. *CLinical Chem.* **1993**, *39*, 424–432.

44. Fourcaud, T.; Ji, J.N.; Zhang, Z.Q.; Stokes, A. Understanding the impact of root morphology on overturning mechanisms: A modelling approach. *Ann. Bot.* **2008**, *101*, 1267–1280. https://doi.org/10.1093/AOB/MCM245.
45. Stubbs, C.J.; Cook, D.D.; Niklas, K.J. A general review of the biomechanics of root anchorage. *J. Exp. Bot.* **2019**, *70*, 3439–3451. https://doi.org/10.1093/JXB/ERY451.

Disclaimer/Publisher's Note: The statements, opinions and data contained in all publications are solely those of the individual author(s) and contributor(s) and not of MDPI and/or the editor(s). MDPI and/or the editor(s) disclaim responsibility for any injury to people or property resulting from any ideas, methods, instructions or products referred to in the content.